Combustion and Flame 198 (2018) 477–489

Contents lists available at ScienceDirect

Combustion and Flame

journal homepage: www.elsevier.com/locate/combustflame

A physics-based approach to modeling real-fuel combustion chemistry – IV. HyChem modeling of combustion kinetics of a bio-derived jet fuel and its blends with a conventional Jet A

Kun Wang[a], Rui Xu[a], Tom Parise[a], Jiankun Shao[a], Ashkan Movaghar[b], Dong Joon Lee[b], Ji-Woong Park[c], Yang Gao[c], Tianfeng Lu[c], Fokion N. Egolfopoulos[b], David F. Davidson[a], Ronald K. Hanson[a], Craig T. Bowman[a], Hai Wang[a,*]

[a] Department of Mechanical Engineering, Stanford University, Stanford, CA 94305-3032, USA
[b] Department of Aerospace and Mechanical Engineering, University of Southern California, Los Angeles, CA 90089-1453, USA
[c] Department of Mechanical Engineering, University of Connecticut, Storrs, CT 06269-3139, USA

ARTICLE INFO

Article history:
Received 30 May 2018
Revised 20 June 2018
Accepted 16 July 2018
Available online 7 August 2018

Keywords:
Bio-derived jet fuel
Jet A
Hybrid Chemistry approach (HyChem)
Fuel blends

ABSTRACT

A Hybrid Chemistry (HyChem) approach has been recently developed for the modeling of real fuels; it incorporates a basic understanding about the combustion chemistry of multicomponent liquid fuels that overcomes some of the limitations of the conventional surrogate fuel approach. The present work extends this approach to modeling the combustion behaviors of a two-component bio-derived jet fuel (Gevo, designated as C1) and its blending with a conventional, petroleum-derived jet fuel (Jet A, designated as A2). The stringent tests and agreement between the HyChem models and experimental measurements for the combustion chemistry, including ignition delay and laminar flame speed, of C1 highlight the validity as well as potential wider applications of the HyChem concept in studying combustion chemistry of complex liquid hydrocarbon fuels. Another aspect of the present study aims at answering a central question of whether the HyChem models for neat fuels can be simply combined to model the combustion behaviors of fuel blends. The pyrolysis and oxidation of several blends of A2 and C1 were investigated. Flow reactor experiments were carried out at pressure of 1 atm, temperature of 1030 K, with equivalence ratios of 1.0 and 2.0. Shock tube measurements were performed for the blended fuel pyrolysis at 1 atm from 1025 to 1325 K. Ignition delay times were also measured using a shock-tube. Good agreement between measurements and model predictions was found showing that formation of the products as well as combustion properties of the blended fuels were predicted by a simple combination of the HyChem models for the two individual fuels, thus demonstrating that the HyChem models for two jet fuels of very different compositions are "additive."

1. Introduction

A vast majority of the 200 million gal/day of jet fuels used worldwide is derived from petroleum, and accounts for ~2% of total global anthropogenic CO_2 emissions [1]. Bio-derived and synthetic jet fuels currently amount to <1% of total jet fuel utilization. The use of alternative jet fuels is projected to reach 6% by 2020. One of the barriers to adopting alternative jet fuels is the current combination of fuel testing, approval, and certification processes, which are expensive and time consuming. As a part of a larger effort to streamline the testing/approval process [2], the current work aims at developing a modeling approach that can reliably predict the combustion chemistry of alternative/conventional fuels and their blends. The current paper is also one of a series of studies centered on the development of a Hybrid Chemistry (HyChem) approach to modeling real-fuel combustion chemistry.

A typical jet fuel is a mixture of thousands of hydrocarbon species. Historically, combustion chemistry modeling of real, multicomponent fuels has been approached through a surrogate fuel approach [3–8]. One of the drawbacks of this approach is that it requires extensive experimentation to validate the surrogate compositions and combustion kinetic models of surrogate components and their kinetic couplings. Moreover, these reaction models are usually large in size with many thermodynamic and kinetic parameters that are empirically estimated.

* Corresponding author.
E-mail address: haiwang@stanford.edu (H. Wang).

https://doi.org/10.1016/j.combustflame.2018.07.012
0010-2180/

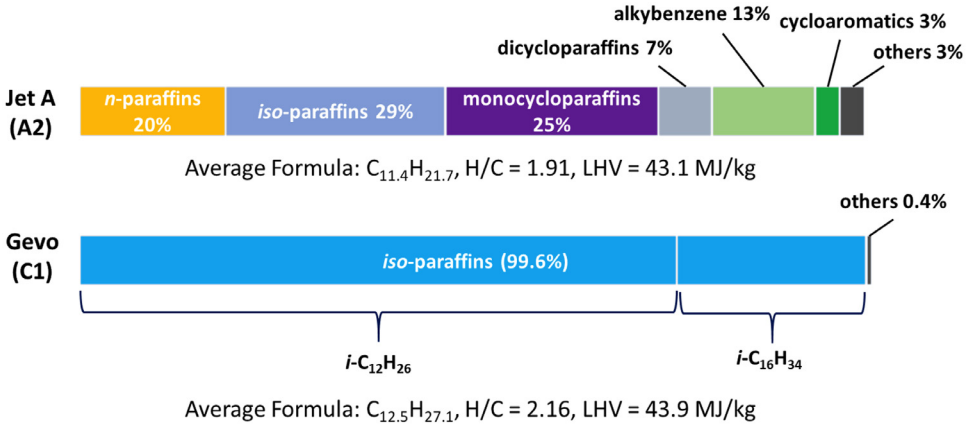

Fig. 1. Comparison of composition and key properties between A2 (POSF10325) and C1 (POSF11498).

In recent studies [9,10], we proposed the alternative HyChem approach to modeling the combustion chemistry of real, multicomponent liquid fuels. Briefly, a HyChem model is comprised of an experimentally constrained lumped fuel (oxidative) pyrolysis submodel and a detailed foundational fuel chemistry submodel that describes the oxidation of H_2/CO/C_1–C_4/benzene/toluene species. As discussed in our earlier study [9], the HyChem approach has many similarities with the lumping approach championed by Ranzi et al. (see, e.g., [11–13]), but it also has two key differences. The development of the HyChem model does not rely on the availability of a detailed reaction mechanism or model to derive the lumped model. Rather, the approach relies on a physical, cause-and-effect understanding and as importantly, advanced diagnostics to reliably achieve model predictability. More importantly, the HyChem approach bypasses the use of surrogate as it seeks to unravel the real-fuel combustion process and properties and advance the modeling capability from these properties directly.

Key assumptions and their justifications have been discussed in [9]. They are:

(1) High-temperature combustion of hydrocarbon fuels sufficiently large in molecular size follows a decoupled, two-step process: fuel pyrolysis first, followed by oxidation of decomposed products.
(2) Fuel decomposition can be described by (experimentally constrained) lumped reaction steps with constant stoichiometric coefficients and pseudo-reaction rate coefficients, which may be justified from a steady-state analysis.
(3) The oxidation of the products of fuel pyrolysis, including C_2H_4, C_3H_6, C_4H_8 (1-butene and *iso*-butene), CH_3, CH_4, H, H_2, C_6H_6 (benzene) and C_7H_8 (toluene), must be treated by detailed modeling because they govern the combustion chemistry properties in most cases.

In the HyChem approach, the lumped fuel pyrolysis and oxidative pyrolysis submodel may be derived directly from detailed time-resolved speciation data from shock tubes and flow reactors. Global combustion properties, including shock tube ignition delay times, laminar flame speeds, non-premixed flame extinction strain rates, are used for testing model accuracy. It was shown that the approach works well for a range of jet and rocket fuels, all of which are multicomponent distillate fuels [10]. The size of a HyChem model is compact, and can be reduced to about 30 species for incorporation into CFD simulations (see, e.g., [14,15]).

Unlike conventional jet fuels, bio-derived fuels often contain a fewer number of hydrocarbon components. The Gevo alcohol-to-jet fuel (designated as the C1 fuel [2]) is such an example. As shown in Fig. 1, a typical conventional jet fuel (POSF10325 – a typical commercial Jet A designated as the A2 fuel [2]) contains several major classes of hydrocarbon compounds; and the number of components is numerous. In comparison, C1 is comprised of almost entirely the highly branched *i*-$C_{12}H_{26}$ and *i*-$C_{16}H_{34}$ (with ~0.4% C_{13}–C_{15} hydrocarbons, which appear to be also highly branched). A comparison for the main properties of the Gevo and A2 fuels is provided in Table S1 of the Supplementary materials (SPM). Additional information can be found in Ref. [2]. The pyrolysis of the A2 fuel produces primarily ethylene (C_2H_4) [10], whereas C1 produces mostly *iso*-butene (*i*-C_4H_8), as will be shown later. Coupled with the fact that C1 is a representative case of a "few-component" fuel, it forms a unique case to test the range of applicability of the HyChem approach. This constitutes the first objective of the study.

Additional objectives stem from the consideration that alternative fuel utilization is likely to start with fuel blending. A logical question that follows is, what is the acceptable level of a bio-derived fuel, such as the C1 fuel that can be blended into a conventional jet fuel without an adverse impact on its combustion properties? From the standpoint of combustion chemistry evaluation, a related question is, do HyChem models that have been developed separately for two blending components still reproduce the combustion chemistry properties of blended fuels by simply combining the two pyrolysis submodels? Thus, the second objective of the current study is to address the above question using a series of A2–C1 blends as examples.

2. Experimental

2.1. Shock tube facilities

Pyrolysis speciation and ignition delay time (IDT) experiments were performed using the Stanford high- and low-pressure shock tubes. Descriptions of these two facilities and the fuel handling protocol can be found in [10]. Three diagnostic methods were used: pyrolysis speciation measurements via laser absorption, IDT measurements via OH* emission and sidewall pressure. Laser absorption measurements employed the Beer–Lambert law, $-\ln[(I/I_0)\lambda] = \sigma_\lambda NL$, to relate the measured absorbance $-\ln[(I/I_0)\lambda] = \sigma_\lambda NL$ to the unknown species concentrations, using measured absorption cross-sections σ_λ. In the experiments to measure C_2H_4 and CH_4 time-histories, where one product dominated the absorbance at a particular wavelength and other species have nearly constant absorbance at this wavelength, a two-wavelength differential method was used to determine the concentration of the dominant absorber. A three-color sensor using Access Laser^{TM} CO_2 gas laser operating at 10.532 and 10.675 µm and a Day-light Solutions^{TM} ECQCL operated at 881.4 cm^{-1} was

used to measure C_3H_6 and *iso*-C_4H_8 concentrations. Further details of the laser absorption method are given in Parise et al. [16].

2.2. Flow reactor facilities

The Stanford flow reactor facility [17] was used to investigate the oxidative pyrolysis kinetics of the jet fuels. The flow reactor is comprised of a vertical 30-cm long and 3-cm diameter quartz reactor tube enclosed in a pressure vessel. The combustion products of a H_2/air flame stabilized on a water-cooled McKenna burner at the base of the reactor provide a hot vitiated flow in which the injected fuel undergoes reaction under near adiabatic conditions. Electric heaters surround the reactor tube to maintain nearly isothermal conditions. A liquid fuel was injected into a vaporizer by a syringe pump before being introduced into the reactor with a nitrogen carrier gas. The reaction products were sampled by a cooled extraction probe that was translated along the reactor centerline using a computer-controlled stepping motor. Gas samples were sent through a heated line to a 4-column micro gas chromatograph (Inficon microGC 3000) for sample analysis. In addition, a non-dispersive infrared analyzer (NDIR) and a paramagnetic analyzer (PMA) were used for real-time measurements of CO, CO_2 and O_2 that could be compared with the GC data. Typical residence times in the reactor were 30 ms. The total uncertainty in concentration is ± 2–5% for most species.

2.3. Flame speed measurements

The laminar flame speed S_u° of A2/air and C1/air mixtures were measured in a counterflow configuration at atmospheric pressure and an unburned mixture temperature $T_u = 403$ K, similar to our previous study [10]. The system included a high-pressure precision pump to meter the liquid fuel and a vaporization chamber in which a quartz nebulizer was used to spray the fuel into a preheated stream of air. Small amounts of silicone oil were added to the fuel to serve as flow tracer. Throughout the fuel-heating path the temperatures were controlled in order to avoid hot spots leading to fuel cracking and cold spots leading to fuel condensation. A double pulsed ND:YAG laser and a high performance 12 bit CCD camera with 1376 × 1040 pixels of resolution were used to acquire Particle Image Velocimetry (PIV) images. The minimum axial velocity along the system centerline just upstream of the flame was defined as a reference flame speed, $S_{u,ref}$, and the maximum absolute value of axial velocity gradient was defined as a local strain rate, K. As K was varying, its effect on $S_{u,ref}$ was recorded, and S_u° was determined through computationally-assisted extrapolation [18]. The 2σ standard deviations in S_u° are indicated with uncertainty bars in relevant figures.

2.4. Experiments of C1 and A2 Blends

Oxidation of several A2–C1 blends was examined in the flow reactor and shock tube facilities. The blended fuels were prepared by volumetrically mixing A2 and C1 fuels with a pipette. Three blends were investigated. They are 20-unit volume of A2 blended with 80-unit volume of C1 (designated as 20A2-80C1), 50A2-50C1, and 80A2-20C1. Note that the molar ratio of a blend is slightly different from the volume ratio, due to differences in the fuel density and mean molecular weight. The flow reactor experiments were conducted under atmospheric pressure and temperature of 1030 K with the equivalence ratio $\phi = 1.0$ and 2.0. The recovered mass balances for hydrogen and carbon exceed 95%, indicating most products are accounted for. The shock tube experiments focused on the formation of C_2H_4, C_3H_6, and *i*-C_4H_8 from the same blends from 1025 to 1325 K at a pressure of 1.2 atm. IDTs for blends of 80A2-20C1 and 50A2-50C1 were also determined in the shock tube. In both facilities, individual A2 and C1 experiments were conducted under similar conditions.

3. Modeling approach

3.1. HyChem model formulation

A HyChem model has been proposed previously for the A2 fuel [10]. The present study focuses on the C1 fuel. While the real C1 fuel has a molecular formula of $C_{12.5}H_{27.1}$, the modeled fuel is assumed to have a formula of $C_{13}H_{28}$ to accommodate the existing chemical kinetics codes. Thus, in the computations, the specification of unreacted mixture compositions relies on matching the mass fraction of the fuel in an experiment, and not the mole fraction. Details of how to match the mass fraction of the fuel can be found in [10]. The standard-state enthalpy of formation was calculated from the LHV value (cf. Fig. 1). The specific heat, entropy, and sensible enthalpy were estimated from a mixture containing 86.49% (mole) *iso*-dodecane and 13.51% *iso*-hexadecane. Additionally, the model formula ($C_{13}H_{28}$) is determined by matching both the H/C ratio and closest integer round-off of an alkane formula. The transport properties of the fuel are determined based on a series of recent studies [19–21] of long-chain normal alkane molecules, assuming the binary diffusion coefficients of the fuel is equal to the diffusion coefficient of a normal alkane molecule of the same carbon number. Therefore, the diffusion coefficients of the C1 fuel are assigned to be those of *n*-tridecane (*n*-$C_{13}H_{28}$).

The stable products considered for C1 decomposition are *i*-C_4H_8, C_3H_6, C_2H_4, CH_4, and H_2. The lumped reactions for C1 pyrolysis/oxidative pyrolysis are written as follows:

$$C_{13}H_{28} \rightarrow e_d(i\text{-}C_4H_8 + \omega_3 C_3H_6 + \omega_2 C_2H_4) + \alpha H + (2-\alpha)CH_3 \quad \text{(R1)}$$

$$C_{13}H_{28} + H \rightarrow H_2 + \Sigma_p \quad \text{(R2)}$$

$$C_{13}H_{28} + CH_3 \rightarrow CH_4 + \Sigma_p \quad \text{(R3)}$$

$$C_{13}H_{28} + OH \rightarrow H_2O + \Sigma_p \quad \text{(R4)}$$

$$C_{13}H_{28} + O_2 \rightarrow HO_2 + \Sigma_p \quad \text{(R5)}$$

$$C_{13}H_{28} + HO_2 \rightarrow H_2O_2 + \Sigma_p \quad \text{(R6)}$$

$$C_{13}H_{28} + O \rightarrow OH + \Sigma_p \quad \text{(R7)}$$

where

$$\Sigma_p = e_a(i\text{-}C_4H_8 + \omega_3 C_3H_6 + \omega_2 C_2H_4) + \beta H + (1-\beta)CH_3$$

Reaction R1 represents the C–C fission in the fuel "molecule", followed by the decomposition of the resulting radical fragments. Reactions R2 through R7 describes the H-abstraction of the fuel "molecule" followed by β-scission of the resulting fuel radical. e_d and e_a are dependent stoichiometric coefficients that may be determined from the independent parameters, α, β, ω_2, and ω_3, through atom balances

$$e_d(4 + 2\omega_2 + 3\omega_3) + 2 - \alpha = 13 \quad (1)$$

$$e_a(4 + 2\omega_2 + 3\omega_3) + 1 - \beta = 13 \quad (2)$$

The physical significance of the independent parameters is self-explanatory. As seen in Table 1, α and β are the numbers of H

Table 1
Independent, stoichiometric parameters and their determination in the C1 HyChem model.

Parameter	Descriptions	Range	Method of determination
α	Number of H-atoms produced in the fuel "C–C fission reaction" (R1) per $C_{13}H_{28}$	[0, 2]	Shock-tube species-time history of i-C_4H_8, C_3H_6, C_2H_4 and CH_4
β	Number of H-atoms produced in the fuel "H-abstraction reaction" (R2) per $C_{13}H_{28}$	[0, 1]	Shock-tube species-time history of i-C_4H_8, C_3H_6, C_2H_4 and CH_4
ω_3	$[C_3H_6]/[i\text{-}C_4H_8]$	$[0, \infty)$	Flow reactor speciation data
ω_2	$[C_2H_4]/[i\text{-}C_4H_8]$	$[0, \infty)$	Flow reactor speciation data

radicals generated in R1 and R2–7, respectively. The corresponding numbers of the methyl (CH_3) radicals are 2–α and 1–β, respectively. The production of H_2 and CH_4 are from the H-abstraction reactions of fuel by H and CH_3 radicals. The parameters ω_2, and ω_3 are the C_2H_4-to-i-C_4H_8 and C_3H_6-to-i-C_4H_8 ratios, respectively.

The stoichiometric coefficients and kinetic rate parameters are derived from species time histories measured in shock tube pyrolysis and flow reactor oxidative pyrolysis of the C1 fuel (see, Table 1). With four independent stoichiometric coefficients and seven rate coefficients to be determined, the problem can be quite well defined given the experimental capabilities available. The pyrolysis model is combined with a detailed foundational fuel model to describe the entire oxidation process. An updated USC Mech II [22] is used here for this purpose. The updates concern mostly the pyrolysis and oxidation of i-C_4H_8 as USC Mech II was not specifically developed to cover that part of the chemistry. The need for and details of the updates are provided in section S2 of SPM. The pyrolysis part of the C1 HyChem model thus developed is also provided in section S2 of the SPM, including the stoichiometric parameters and kinetic rate parameters. The entire reaction models and their associated thermochemical and transport data are available for download from the HyChem website.

3.2. Blended A2–C1 HyChem model

A blended HyChem model was created by simply combining the (experimentally constrained) lumped pyrolysis models of A2 and C1 with their common foundational chemistry model. As will be discussed later, neither the global combustion properties measured nor the experiments on fuel blends were used to determine the coefficients and rate parameters of the C1 model. The mass density is 0.804 g/cm^3 for A2 and 0.761 g/cm^3 for C1. These values are used to calculate the mole ratio of A2 to C1 from the pre-blending fuel volume fraction.

3.3. Computational details

The Chemkin code [23] was used for kinetic modeling. The computed IDT was defined as the time to reach the maximum OH* production rate in an adiabatic, isochoric calculation. PREMIX [24] with multicomponent transport and thermal diffusion was employed for calculation of S_u°.

4. Results and discussions

4.1. Pyrolysis/oxidative pyrolysis experiments and HyChem model development

The stoichiometric parameters and rate coefficients of the C1 HyChem model are constrained and determined by the speciation data obtained from both the shock tube and flow reactor facilities. Representative species profiles in the shock tube pyrolysis of C1 are shown in Fig. 2. Under the conditions tested, the most important products are i-C_4H_8, followed by C_3H_6, C_2H_4, and CH_4. For the experiment at 1070 K, the product concentrations continue to rise within 2 ms of measurement time, whereas at 1317 K, they level off as nearly all fuel has been consumed in the first 0.1 ms. The types of data shown here as well as the flow reactor speciation data to be discussed later were used to derive the HyChem model parameters in an inverse problem. Obviously, the model reproduces the experimental data well.

Yields of the two dominant products, i-C_4H_8 and C_3H_6 during C1 pyrolysis are shown at the reaction time of 0.5 ms in the left panel of Fig. 3. For comparison, the two most important species in A2 pyrolysis, C_2H_4 and CH_4, are also shown in Fig. 3 (the right panel). Clearly, C1 produces distinctively different species from A2. These differences determine the somewhat different combustion properties of the two fuels, as will be discussed later. It has been shown in [10] that over the range tested, pressure exhibits little to no impact on the product distributions.

Figure 4 depicts the mole fraction profiles of key species measured during flow reactor oxidation of C1 at 1030 K and 1 atm. The fuel concentrations were measured by tracking fuel-relevant GC peaks. A comparison between C1 and A2 flow reactor experiments for the fuel conversion and major product formation is provided in Fig. S4 of the SPM. Under the condition tested, C1 decomposes faster than A2. The observed product distribution in C1 is consistent with the shock tube observations, with i-C_4H_8 being the dominant species, followed by H_2, C_3H_6, CH_4, and C_2H_4. As shown in the right panel of Fig. 4, several secondary species are also formed, including C_2H_6 (ethane), a-C_3H_4 (allene), and p-C_3H_4 (propyne). The measurements and modeling for several other secondary products with concentrations less than 20 PPM, including 1-C_4H_8 (1-butene), C_6H_6 (benzene), $C_6H_5CH_3$ (toluene), C_2H_2 (acetylene), C_5H_6 (cyclopentadiene), are provided in Fig. S5 of the SPM. Key information from the flow reactor experiments, including the ratios of C_2H_4 and C_3H_6 to i-C_4H_8 and the absolute concentrations of CH_4 and H_2, were used to derive the parameters of C1 HyChem model.

The rapid rise measured for the concentrations of many species during the early stage of reaction was caused by finite-rate fluid mixing at the reactor entrance. For this reason, simulations start at 3 ms with the species concentrations measured at that reaction time used as the initial condition. This approach was discussed in an earlier experimental and modeling study of n-dodecane pyrolysis and oxidation in the same flow reactor [17] and used in all previous HyChem work [9,10]. As shown in Fig. 4, the HyChem model results are in good agreement with the experimental data. The slight overprediction of the C1 concentration at 3 ms and in the mid-range of the reaction time stems from one of the HyChem model assumptions wherein all unaccounted species are lumped into the fuel.

4.2. Testing the model against global combustion properties

The thus developed C1 HyChem model was tested against the global combustion properties. The effects of temperature (950–1550 K), pressure (1–40 atm), and equvelence ratio (0.4 and 1.0) on IDT were examined in the shock tube. Representative results are presented in Fig. 5 at two pressures. A more complete experimental dataset as well as the HyChem model predictions are provided in Fig. S6 of the SPM. As these comparisons show, the C1 HyChem model succesfully predicts the IDT data. For comparison, the IDT of A2 under comparable conditions are also presented

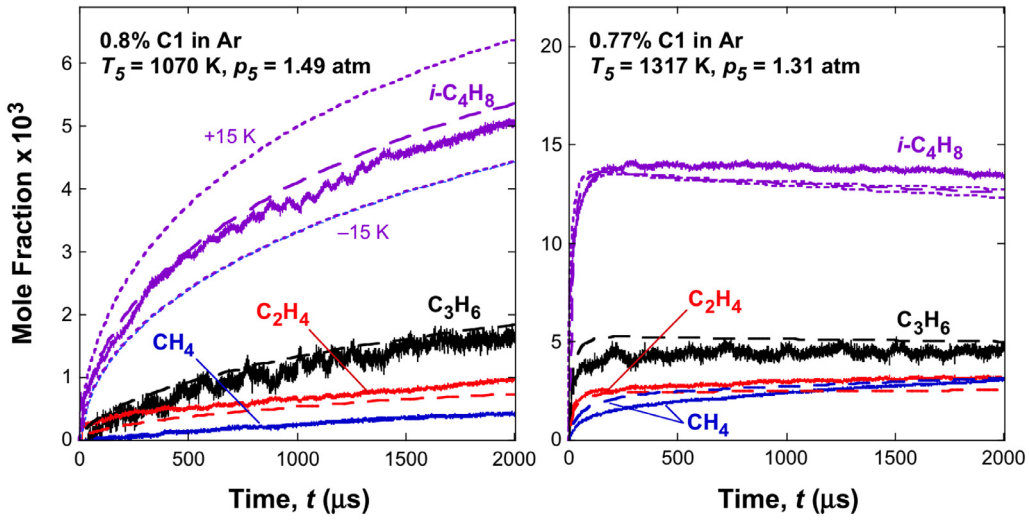

Fig. 2. Experimental (solid lines) and computed (long dashed lines) species time histories during the pyrolysis of C1 in shock tube under two conditions (T_5 and p_5 are the post-reflected shock temperature and pressure, respectively). Short dashed lines: computed, ±15 K temperature sensitivity on i-C_4H_8. In the left panel, the predicted and experimental CH_4 profiles overlap with each other.

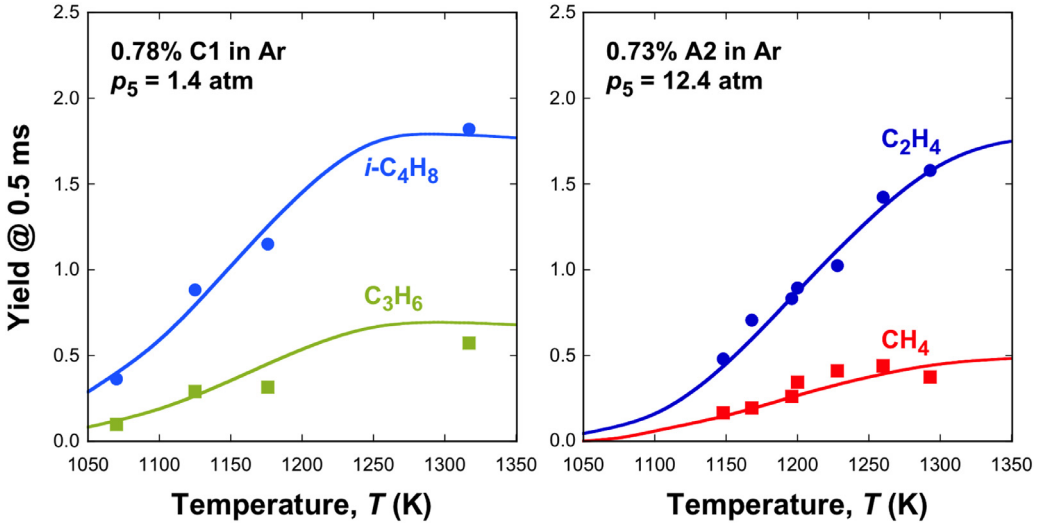

Fig. 3. Measured (symbols) and computed (lines) yields of the dominant decomposition products during the pyrolysis of C1 (the left panel) and A2 (the right panel) in shock tube. The data in the right panel are taken from [10].

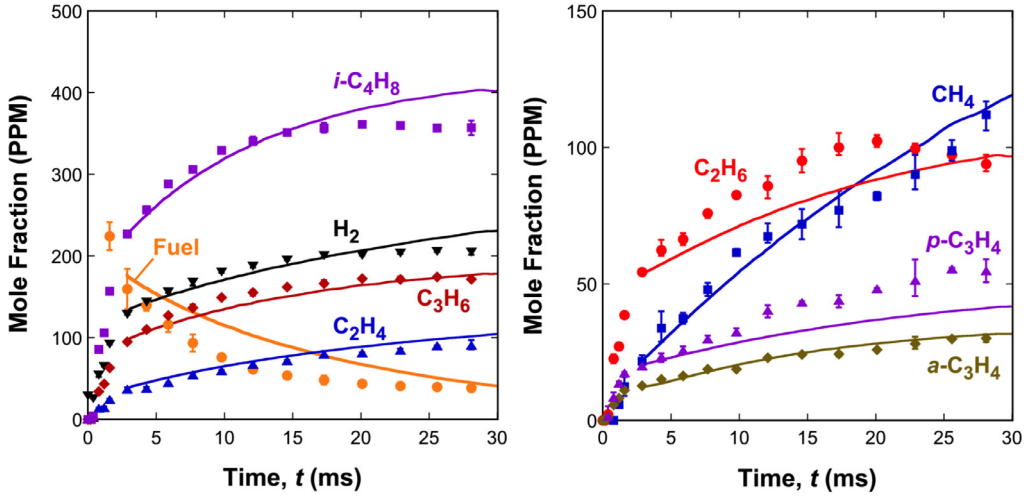

Fig. 4. Experimental (symbols) and computed (lines) species concentrations during oxidative pyrolysis of C1 in flow reactor at T = 1030 K, p = 1 atm, input fuel concentration = 305 PPM fuel, ϕ = 1. See Table S3 in the SPM for the computational initial condition.

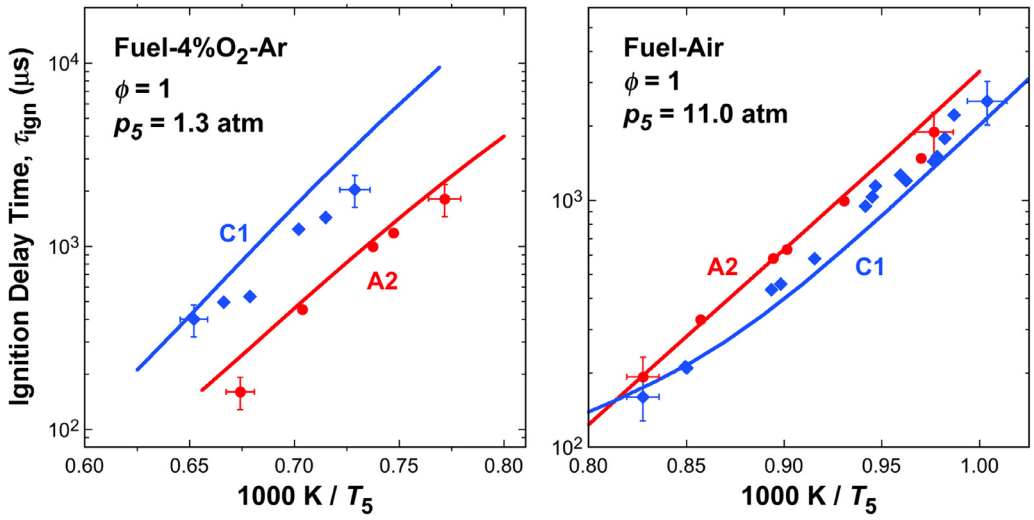

Fig. 5. Experimental (symbols) and computed (lines) ignition delay times of Jet A (A2) and Gevo (C1) in 4% O_2 diluted by Ar (the left panel), and in air (the right panel). The error bars are estimated experimental uncertainties (20% in the ignition delay and 1% in the temperature).

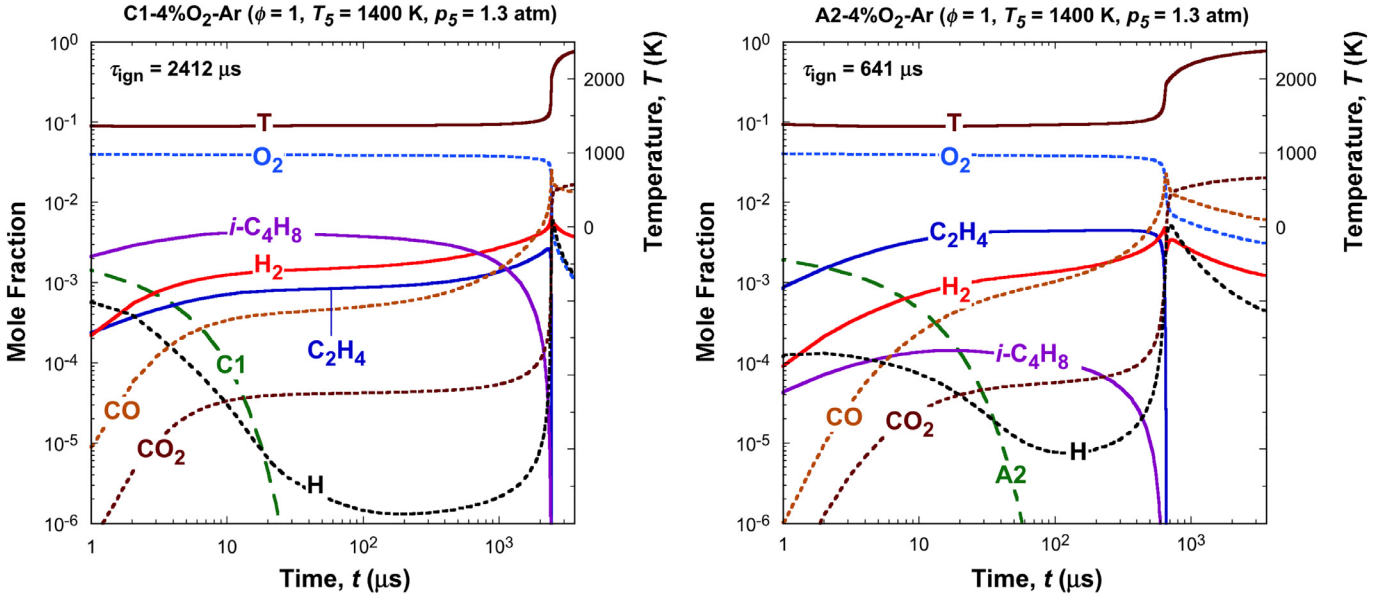

Fig. 6. Mole fraction profiles computed for the oxidation of C1 (the left panel) and A2 (the right panel), both at 1400 K.

in Fig. 5. Clearly, the IDT of A2 and and C1 exhibit different responses to temperature. Above 1250 K (the left panel of Fig. 5), A2 ignites faster than C1; below 1250 K (the right panel of Fig. 5), C1 has shorter IDT. Analyses show that the observed difference can be explained by the rate of fuel decomposition versus the rate of oxidation of the resulting decomposition products. Above 1250 K, fuel decomposition is fast for both A2 and C1. Under this condition, C1 has a longer IDT than A2 because the oxidation of i-C_4H_8 is slower than that of C_2H_4, owing to the fact that the *iso*-butenyl (i-C_4H_7) is a resonantly stabilized species. Its reaction with O_2 is substantially slower than the reaction between vinyl (C_2H_3) and O_2. The slower ignition of C1 is consistent with an earlier observation [25] that branched-chain hydrocarbons tend to require a longer time to ignite than normal-chain hydrocarbons. Below 1250 K, however, the overall reaction rate is limited by thermal decomposition of the parent fuel. Because C1 decomposes faster than A2, its overall induction time shortens as compared to A2.

To illustrate the above points, Fig. 6 presents the mole fraction profiles of selected species computed for A2 and C1 oxidation at 1400 K and 1.3 atm. The fuel profiles indicate C1 is consumed at ~20 μs and A2 is depleted at ~60 μs, while the IDT for C1 and A2 are ~2412 μs and 641 μs, respectively. In both cases, the time scales of fuel decomposition are substantially smaller than IDT, and thus the disparity in the oxidation rates between i-C_4H_8 and C_2H_4 dictates the induction time. At a lower temperature of 1050 K, however, the thermal decomposition of the fuel is rate limiting, as shown in Fig. 7. Under the condition shown, fuel decomposition takes up more than 90% of the total time to ignition; the fuels themselves are present as the dominant species during almost the entire ignition process. As the overall rate of C1 pyrolysis is faster than A2, the IDT of C1 becomes shorter than that of A2. Overall, the effects of the diluent (Ar versus N_2) and reactant concentration are found to be small for the difference in the ignition-delay observed between the A2 and C1 fuel.

The fact that towards low temperatures (e.g., the condition as shown in Fig. 7) the HyChem approach still reproduces the ignition delay time of both fuels (*cf.*, the right panel of Fig. 5) suggest that some of the key assumptions of the HyChem approach can be relaxed. Specifically, HyChem assumes that (a) the fuel decomposition is not rate limiting, and (b) the oxidation of the decomposed

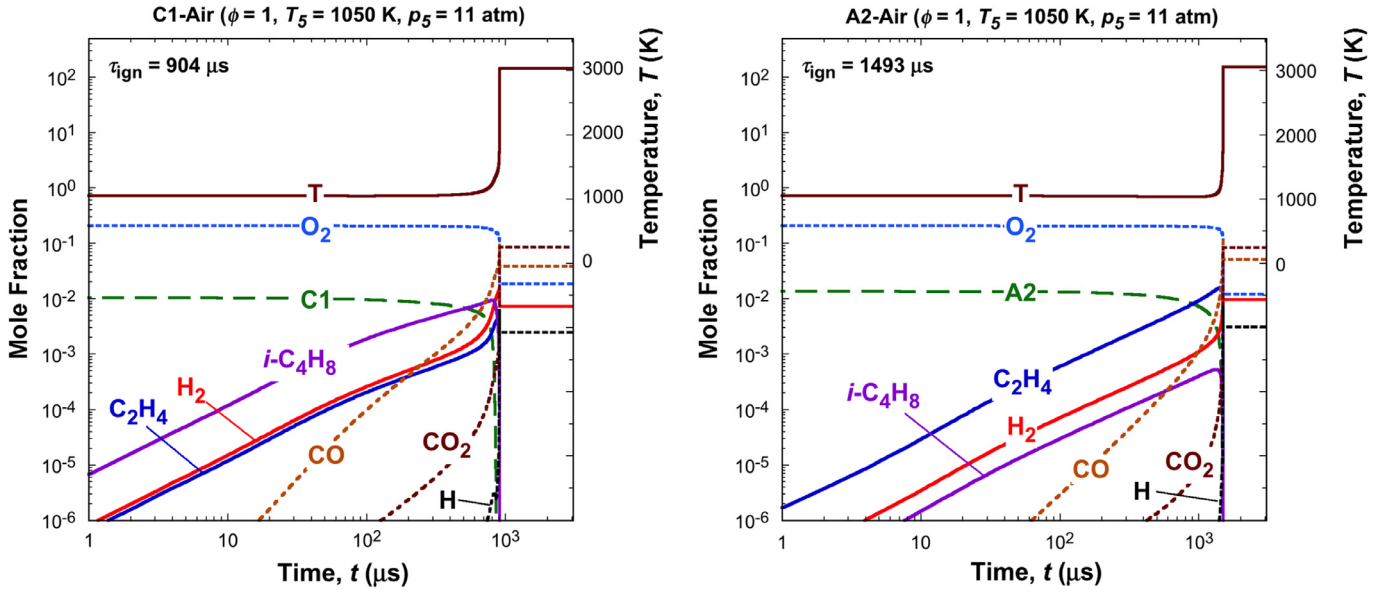

Fig. 7. Mole fraction profiles computed for the oxidation of C1 (the left panel) and A2 (the right panel), both at 1050 K.

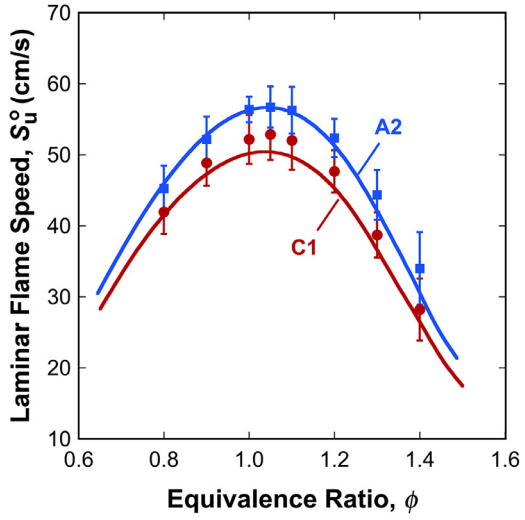

Fig. 8. Measured (symbols) and simulated (lines) laminar flame speeds of A2/air and C1/air mixtures ($T_u = 403$ K, $p = 1$ atm).

products must be rate limiting (i.e., assumptions 2 and 4 as stated in Ref. [9]). These two related assumptions appear to be unnecessary. Even if the fuel decomposition is rate limiting, the decoupled treatment of fuel pyrolysis followed by decomposed product oxidation appears to be valid under all conditions tested thus far.

The experimental S_u^o of C1 flames are lower than those of A2 over the range of ϕ tested, as shown in Fig. 8, again due to the fact that the flame propagation is largely controlled by the heat release rate and, hence, the oxidation rate of the decomposed products. While the A2 model accurately predicts the experimental data as shown in the ealier study [10], the C1 model slightly underpredicts the measured S_u^o. Sensitivity analysis suggests that the cause for the discrepancy is the foundational fuel chemistry model, especially in the reactions associated with i-C_4H_8 and i-C_4H_7. Tests of other foundational fuel chemistry models were made, including the more recent Aramco model (V2.0) [26], but none were able to yield a better agreement than what is seen in Fig. 8 using the original or updated USC mech II.

4.3. A2–C1 blends

The measurements and HyChem predictions of the five sets of flow reactor experiments are presented in Fig. 9. The uncertainty bars represent data scatter over at least four measurements. Good reproducibility was achieved during the experiments. Again, to avoid the mixing effects in the entrance of the flow reactor, simulations were initiated at around 3 ms of reaction time. All species measured at that reaction time were used as input, which is provided in Table S4 of the SPM. Again, the small mismatch of the A2 and C1 fuel concentrations at 3 ms is the result that the species not accounted for in the HyChem model are lumped into the fuel, in these cases, proportionally between A2 and C1.

Similar to the neat fuel results, both the model predictions and experiment show that the fuel decay of C1 in the blends is faster than A2 under comparable conditions. Furthermore, the decomposition rate of each fuel scales with blending mole ratios relative to the neat fuels. This indicates that one fuel in the blends has no or negligible impact on the decomposition of the other. Most of the products exhibited the same behavior. Neat C1 produces mostly i-C_4H_8; the blends produce progressively less i-C_4H_8 as the amount of C1 is reduced in the blends. Quantitatively, the i-C_4H_8 yield in each blend is proportional to the C1 mole ratio in the blend. Other products examined include C_3H_6, H_2, CH_4, and 1-C_4H_8, all of which showed behaviors identical to i-C_4H_8. Kinetic coupling is observed, however, in C_2H_4 production. The blended HyChem model predicts this coupling as well as the products that show no coupling, suggesting that the observed kinetic coupling occurs because of changes in the radical pool concentration, as the fuel coupling is not considered in the blended model.

Figure 10 shows the impact of stoichiometry by doubling the fuel input. With the higher fuel input, more complex chemistry is expected. Nevertheless, the same conclusion can be drawn from fuel decay and product time profiles. The only exception again is C_2H_4 formation, where kinetic coupling is observed. Nevertheless, the blended HyChem model captures the observed feature. Overall, the flow reactor experiments show that the formation of products other than C_2H_4 is proportional to the blending molar ratios of the neat fuels.

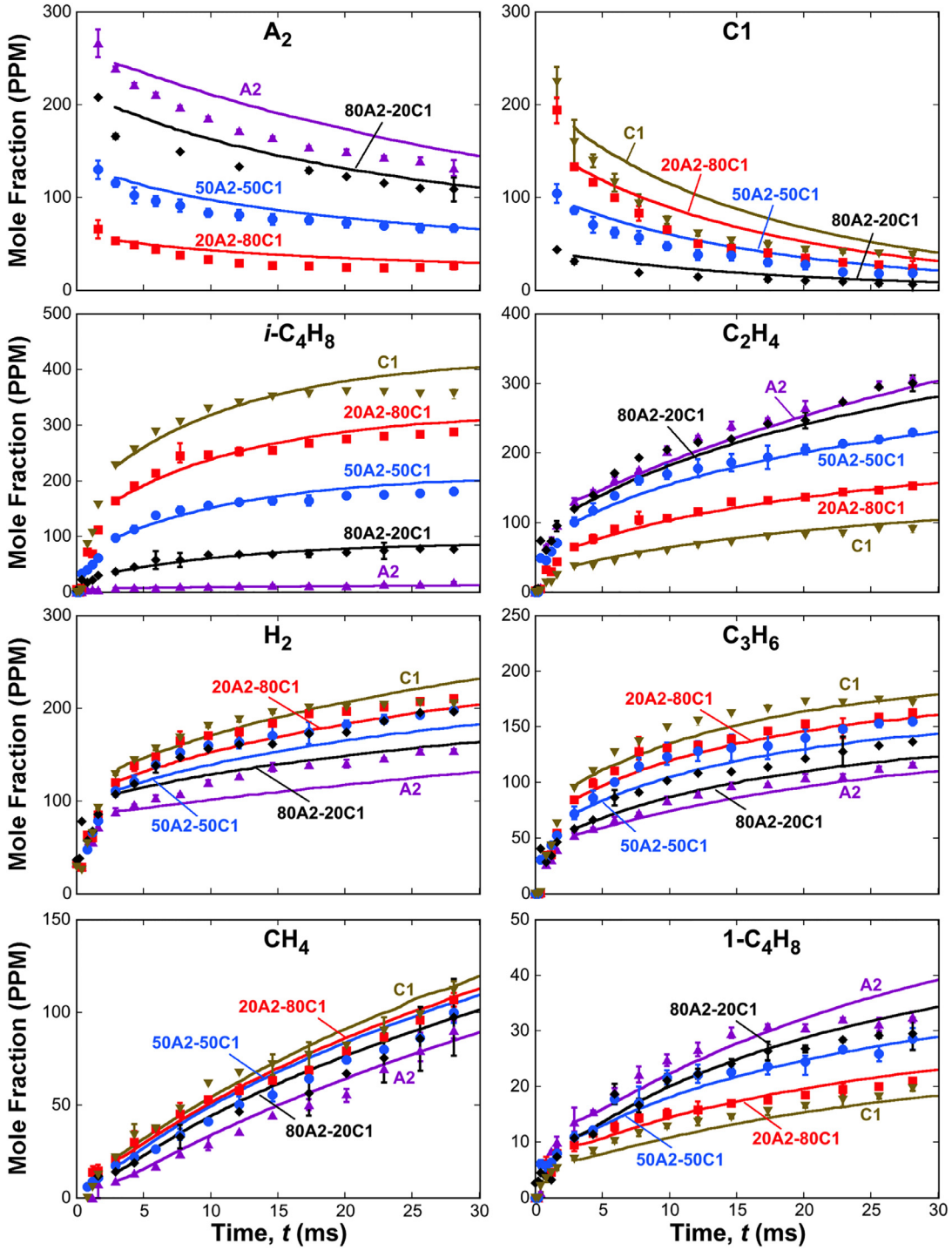

Fig. 9. Experimental (symbols) and HyChem predictions (lines) of the oxidative pyrolysis of neat and blended A2–C1 fuels in the flow reactor (Operating conditions: $T = 1030$ K, $p = 1$ atm, $\phi = 1.0$, average initial fuel mole fraction = 310 (± 5) PPM. 20A2-80C1 designates 20-unit volume A2 blended with 80-unit volume of C1). For the simulation, the initial species concentrations of all the mixtures (at 3 ms) are taken from the measured values with the missing carbon lumped into the fuel proportionally. See Table S4 of the SPM for the computational initial conditions.

4.4. Blend speciation from shock-tube experiments

Shock tube pyrolysis experiments measured the formation of three major products, C_2H_4, C_3H_6, and i-C_4H_8, over the temperature range from ~1025 to 1325 K, in the blends as well as neat fuels. The measurements and model predictions are shown in Fig. 11. All the measurements are reported at 2 ms reaction time. The data exhibit some scatter, but the overall trends are clear. C_2H_4 and i-C_4H_8 are the major products in A2 and C1 fuels, respectively. Their formation in the blends is closely related to the mole ratios of the individual fuels. While the C_2H_4 and i-C_4H_8 formation in all fuels is very sensitive to temperature, the C_3H_6 generation

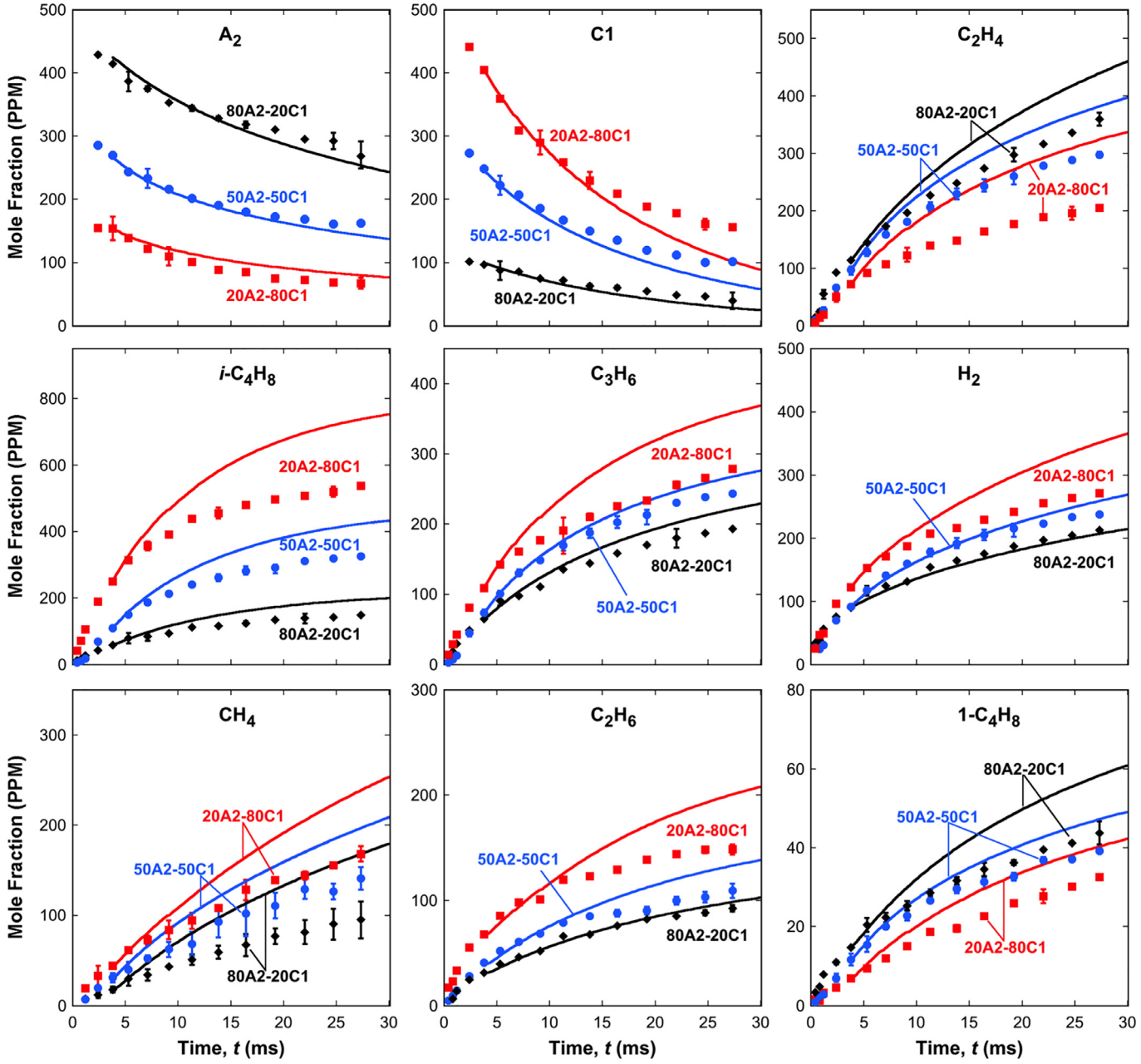

Fig. 10. Experimental (symbols) and HyChem predictions (lines) of of the oxidative pyrolysis of blended A2-C1 fuels in the flow reactor (Operating conditions: $T = 1030$ K, $p = 1$ atm, $\phi = 2.0$, average initial fuel mole fraction = 606 PPM). For the simulation, the initial species concentrations of the 80A2-20C1 and 50A2-50C1 mixtures (at 3 ms) are taken from the measured values with the missing carbon lumped into the fuel proportionally; and those of the 20A2-80C1 mixture are directly taken from the measured values. See Table S4 of the SPM for the computational initial conditions.

showed only weak dependence on temperature. The blended HyChem model for A2–C1 provided an overall good predictions of these speciation data.

4.5. Ignition delay time of A2–C1 blends

IDTs for the A2–C1 blends were also measured in the shock tube at temperatures from 1200 to 1500 K. The measurements and predictions are shown in Fig. 12. As discussed earlier, under these high temperature conditions, the ignition process is largely governed by the oxidation of the decomposed products. Because C_2H_4 oxidation is faster than i-C_4H_8, neat A2 has a shorter IDT than the neat C1, while the IDT of the blended fuels lies between those of the two neat fuels, decreasing with less A2 or increasing with more C1 in the blends. The experimental data show some scatter, yet the trend of ignition delay is clear. The blended HyChem model captures this trend.

Quantitatively, the C1 model over-predicts the C1 ignition delay data by 20–30%; and thus the combined model also overpredicts the ignition delays of the blends to an extent. On the other hand, the experimental values of the A2–air and 80A2-20C1–air mixtures are equal, at least within the data scatters, though a larger ignition delay time is expected for the 80A2-20C1 mixture under comparable conditions. As discussed in [10], the kinetic rate uncertainty of USC Mech II is the largest source of uncertainty in the HyChem model. For example, the rate uncertainty of USC Mech II can impact the ignition delay predictions for the A2 fuel by as much as a factor of three. Here we conduct the same sensitivity analysis as

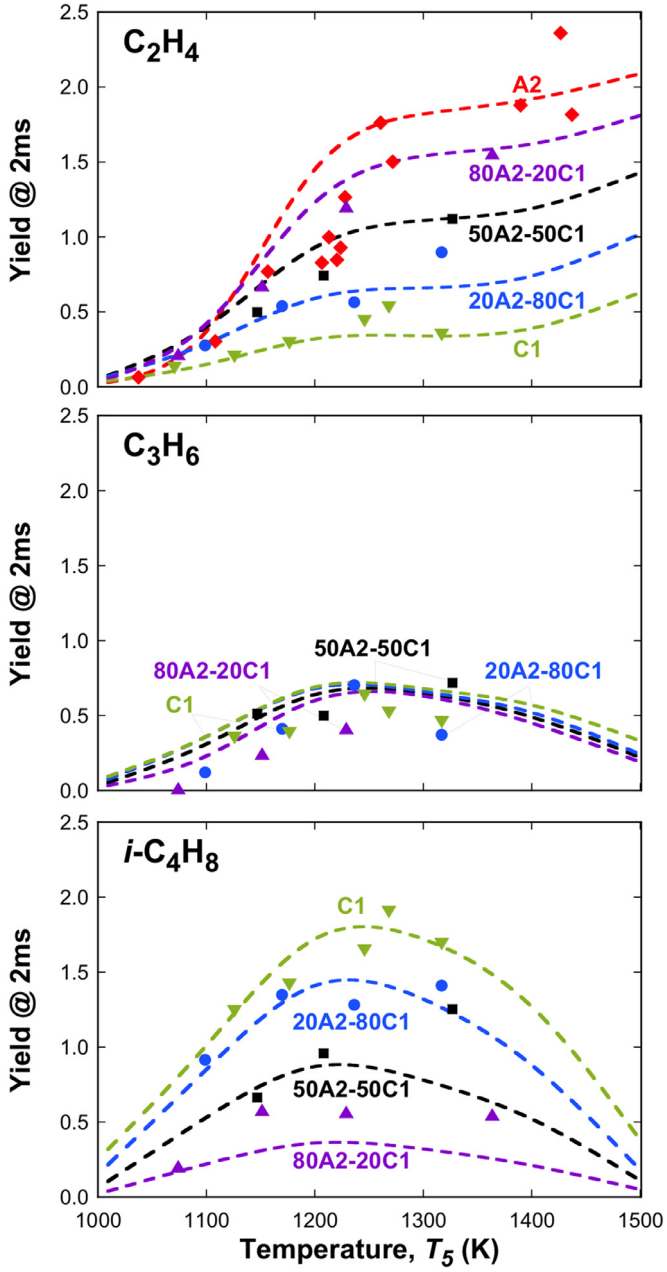

Fig. 11. Experimental (symbols) and HyChem predictions (dashed lines) of ethylene (C_2H_4), propene (C_3H_6), and *iso*-butene (i-C_4H_8) in the pyrolysis of neat and blended A2–C1 fuels in the shock tube (Operating conditions: 0.4% fuel in Ar, $p_5 = 1.2$ atm).

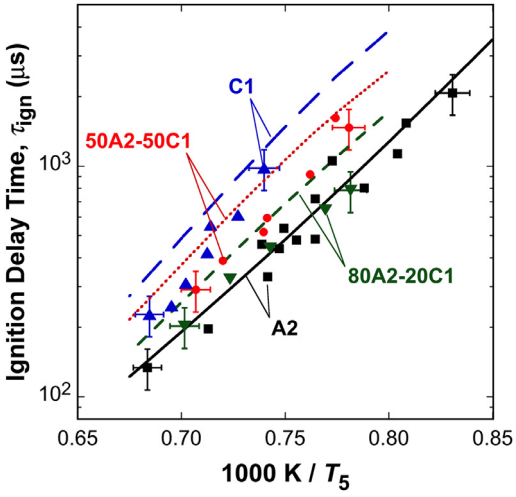

Fig. 12. Experimental (symbols) and HyChem model predictions (lines) of ignition delay time of neat and blended A2–C1 fuels (Operation conditions: fuel in air, $p_5 = 0.56$ atm, $\phi = 1.0$). The error bars are estimated experimental uncertainties (20% in the ignition delay and 1% in the temperature).

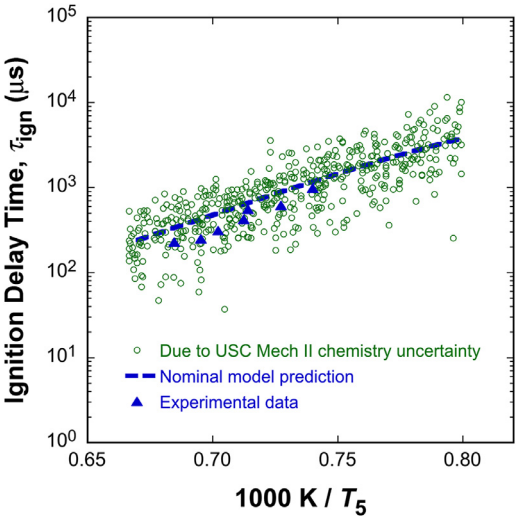

Fig. 13. Sensitivity of HyChem model ignition delay time prediction of C1/air mixture at $p_5 = 0.56$ atm and $\phi = 1.0$ condition.

described in [10], in which 500 random samples of reaction models are generated, and the rate constant of each reaction in USC Mech II is randomly perturbed within its uncertainty. The result is shown in Fig. 13 for C1/air mixture under the same condition as that of Fig. 12. It is seen that the rate uncertainty of USC Mech II can lead to as much as an order of magnitude variations on the ignition delay time prediction. Figure 14 shows a ranked sensitivity spectrum computed for C1/air mixture at the initial temperature of 1400 K and the same pressure and equivalence ratio. There is one fuel-specific reaction (R2) shown in the ranked spectrum, but the sensitivity coefficient value is relatively small. The most important reaction is $H + O_2 = OH + O$, which dictates the radical build-up process, followed by several reactions related to CH_3 and H radicals and i-C_4H_8 molecule. The sensitivity spectrum suggests that the reaction rates and uncertainties of small hydrocarbons in USC Mech II is likely the cause for the experiment-model discrepancy seen in Fig. 12, given that the pyrolysis and oxidation chemistry of i-C_4H_8 is even less certain than those of C_2H_4.

5. Mechanism reduction

HyChem models of C1 with 119-species and A2/C1 mixtures with 120-species are systematically reduced to obtain compact reduced models that are computationally efficient for large-scale flame simulations. Model reduction is based on reaction states sampled from auto-ignition and perfectly stirred reactors (PSR) covering the pressure range of 0.5–30 atm, equivalence ratio of 0.5–1.5, inlet temperature of 300 K for PSR, and initial temperature of 1000–1600 K for auto-ignition, and a number of A2/C1 blends with 0%, 20%, 50%, 80%, and 100% (mole) of A2. It has been found that the thus-reduced models are applicable to different types of combustion phenomena including premixed flame propagation and flame extinction [27].

A skeletal reduction is first performed based on the method of directed relation graph (DRG) [28] and DRG-aided sensitivity analysis (DRGASA) [29], followed by a time-scale based reduction

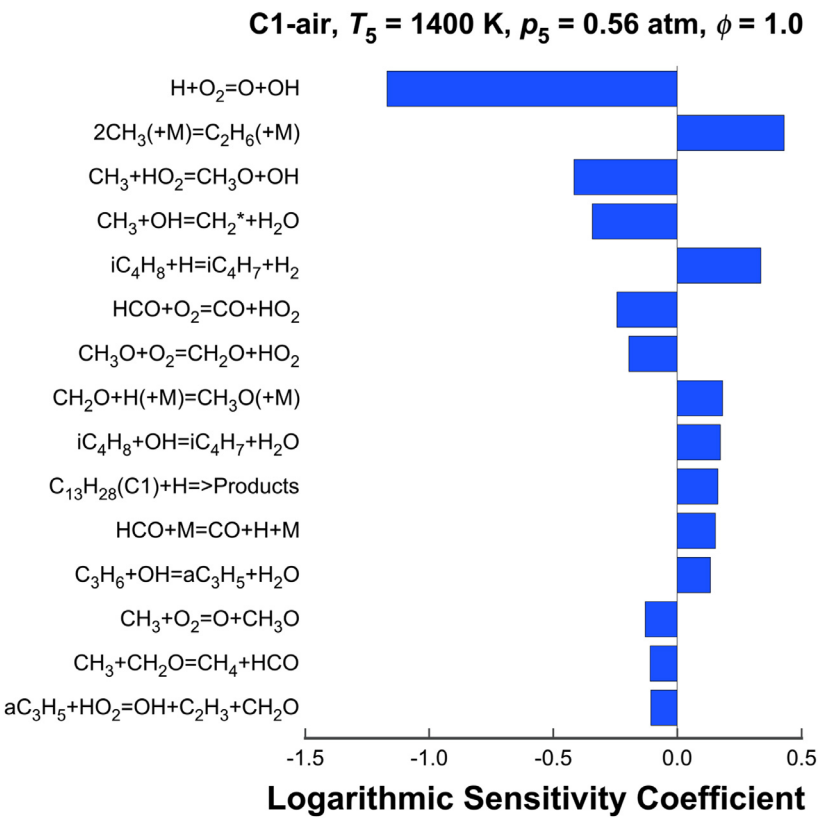

Fig. 14. Ranked logarithmic sensitivity coefficients of the ignition delay time of C1–air mixture at an initial temperature of 1400 K, an initial pressure of 0.56 atm, and equivalence ratio of 1.0.

using the linearized quasi steady state approximations (LQSSA). During skeletal reduction, DRG first maps the species couplings to a graph, and the species important to selected starting species are then identified through a recursive graph search. The H atom is selected as the starting species in the present study with a threshold error tolerance of 0.3 to control the worst-case reduction error, resulting in 93- and 99-species skeletal models for C1 and A2/C1 mixtures, respectively. Next, DRGASA is performed with target parameters being ignition delay and residence time at several points near PSR extinction.

Figure 15 shows the reduction curves of DRGASA for C1 and A2/C1 blends, respectively. It is seen that the number of species in the skeletal model decreases rapidly for error tolerances smaller than about 0.2, and any additional species removal results in rapid growth in the worst-case reduction error. By using an error threshold of 0.22 in DRGASA, a 42-species skeletal model for C1 and a 51-speices skeletal models for A2/C1 mixtures are obtained.

LQSSA is then applied to further reduce the skeletal models. Using the same reaction states sampled for the skeletal reduction, 11-species for C1 and 12-species for A2/C1 blends are identified as globally valid quasi steady state (QSS) species using a method based on computational singular perturbation (CSP) [30]. The final reduced models consist of 31 species for C1 and 39 species for A2/C1 blends. The QSS species are removed from the transport equations with their concentrations being analytically solved using internal algebraic equations [31]. The approach ensures element conservation as demonstrated in Ref. [32]. Both the skeletal and reduced models are available for download at the HyChem website. They include both the models for the C1 fuel only and for A2/C1 blends.

Figure 16 shows the selected validation results of 50%/50% of the A2/C1 blends comparing the skeletal and reduced models to the detailed model for ignition delay, PSR extinction, and laminar

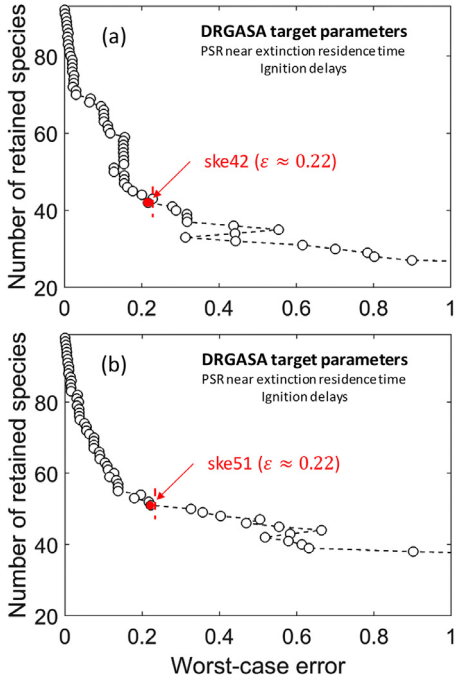

Fig. 15. Number of retained species as a function of the user-specified relative error tolerance in DRGASA for (a) C1 and (b) A2/C1 blends.

flame speed. The worst-case error is approximately 9% for ignition delay, 6% for PSR extinction residence time, and 2.7 cm/s for flame speed. Similar agreement is observed for lean and rich mixtures ($\phi = 0.5$–1.5) for C1 ignition delay and PSR extinction, as well as

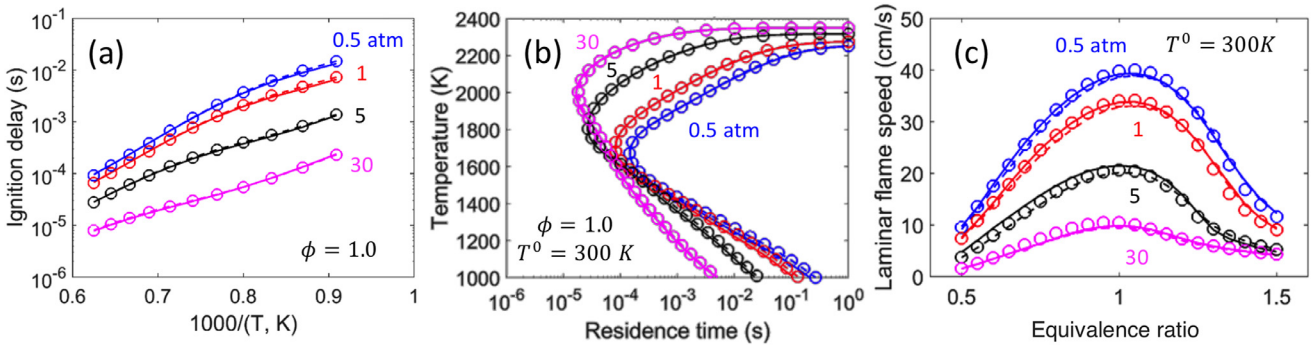

Fig. 16. Selected validation of the skeletal and reduced models for (a) ignition delay, (b) PSR extinction, and (c) laminar flame speed with free stream temperature of 300 K for 50%/50% of the A2/C1 mixture. Detailed: solid lines, skeletal: dotted lines, reduced: symbols.

the A2/C1 blends. Additional test results are shown in section S5 of the SPM (Figs. S7–S13).

6. Conclusions

The present work demonstrated the use of the HyChem approach for the combustion chemistry of an alternative, bio-derived jet fuel (C1), and its comparison with the conventional, petroleum-based jet fuel (A2). Flow reactor experiments revealed that C1 decomposes faster than A2; both the flow reactor and shock tube experiments showed that C1 produces mostly i-C_4H_8 rather than C_2H_4. The ignition delay time of C1 was determined to be longer than that of A2 at high temperatures (above 1250 K), stemming from the difference in the oxidation rates of i-C_4H_8 and C_2H_4. At lower temperatures (below 1250 K) on the other hand, fuel decomposition becomes rate limiting and C1 was found to ignite faster than A2. The laminar flame speeds of A2/air mixtures were determined to be higher than those for C1/air mixtures over a fairly wide range of equivalence ratios. The overall agreement between the HyChem model predictions and experiment was shown to be satisfactory. The fact that the HyChem model developed from species time profile data can predict ignition delay and laminar flame speed data for the same fuel, suggests that the approach is robust and can lead to accurate predictions of combustion properties outside the range of condition where the model is derived.

One of the key objectives of the present study was to investigate whether the HyChem models developed individually for two drastically different fuels could be simply combined to model the combustion behaviors of the blends of the same two fuels. Pyrolysis, oxidation, and ignition delay time measurements were conducted for several blends of the A2 and C1 fuels in both flow reactor and shock tube. A “linear blending rule” was observed for the fuel decay as well as the formation of most of the products with respect to the blending molar ratios of the fuels. The blended HyChem model predicts the experimental observations well, showing that HyChem models can be “additive.” In a broader context, HyChem models currently available for the A2 and C1 fuels may be sufficient for describing the combustion behaviors of all neat or blended jet fuels as long as the dominant fuel decomposition products are C_2H_4, i-C_4H_8, or both.

Acknowledgments

This research was funded by the Air Force Office of Scientific Research under grant numbers FA9550-14-1-0235 (CTB, RKH and HW), FA9550-16-1-0195 (CTB, RKH and HW), FA9550-15-1-0409 (FNE), and FA9550-15-1-0496 (TL). The work was also supported by the National Aeronautics and Space Administration (NASA) under agreement numbers NNX15AV05A (HW) and NNX15AU96A (TL) and by the Federal Aviation Administration Office of Environment and Energy as a part of ASCENT Projects 26 and 35 under FAA Award Numbers 13-CAJFE-SU-006 (HW) and 13-C-AJFE-SU-016 (RKH). Any opinions, findings, and conclusions or recommendations expressed in this material are those of the authors and do not necessarily reflect the views of the FAA or other ASCENT sponsors.

Supplementary materials (SPM) contents

The SPM contain the properties of A2 and C1 fuels (S1), the fuel pyrolysis part of the HyChem model for C1 (S2), updates to USC Mech II (S3), initial condition of flow reactor simulations (S4), and additional test results for the skeletal and reduced reaction models (S5).

Reaction models, including the skeletal and reduced models, can be downloaded from https://web.stanford.edu/group/haiwanglab/HyChem/Index.html.

Supplementary materials

Supplementary material associated with this article can be found, in the online version, at doi:10.1016/j.combustflame.2018.07.012.

References

[1] J.J. Conti, P.D. Holtberg, J. Beamon, A.M. Schaal, J. Ayoub, J.T. Turnure, Annual energy outlook 2014, US Energy Information Administration, (2014).
[2] M. Colket, J. Heyne, M. Rumizen, M. Gupta, T. Edwards, W.M. Roquemore, G. Andac, R. Boehm, J. Lovett, R Williams, Overview of the national jet fuels combustion program, AIAA J. 55 (2017) 1087–1104.
[3] A. Violi, S. Yan, E. Eddings, A. Sarofim, S. Granata, T. Faravelli, E. Ranzi, Experimental formulation and kinetic model for JP-8 surrogate mixtures, Combust. Sci. Technol. 174 (2002) 399–417.
[4] F.L. Dryer, Chemical kinetic and combustion characteristics of transportation fuels, Proc. Combust. Inst. 35 (2015) 117–144.
[5] T. Edwards, M. Colket, N. Cernansky, F. Dryer, F. Egolfopoulos, D. Friend, E. Law, D. Lenhert, P. Lindstedt, H. Pitsch, Development of an experimental database and kinetic models for surrogate jet fuels, 45th AIAA Aerospace Sciences Meeting and Exhibit (2007), p. 770.
[6] W.J. Pitz, C.J. Mueller, Recent progress in the development of diesel surrogate fuels, Prog. Energy Combust. 37 (2011) 330–350.
[7] S. Dooley, S.H. Won, J. Heyne, T.I. Farouk, Y. Ju, F.L. Dryer, K. Kumar, X. Hui, C.J. Sung, H. Wang, M.A. Oehlschlaeger, V. Iyer, S. Iyer, T.A. Litzinger, R.J. Santoro, T. Malewicki, K. Brezinsky, The experimental evaluation of a methodology for surrogate fuel formulation to emulate gas phase combustion kinetic phenomena, Combust. Flame 159 (2012) 1444–1466.
[8] S. Dooley, S.H. Won, M. Chaos, J. Heyne, Y. Ju, F.L. Dryer, K. Kumar, C.J. Sung, H. Wang, M.A. Oehlschlaeger, R.J. Santoro, A jet fuel surrogate formulated by real fuel properties, Combust. Flame 157 (2010) 2333–2339.
[9] H. Wang, R. Xu, K. Wang, C.T. Bowman, D.F. Davidson, R.K. Hanson, K. Brezinsky, F.N. Egolfopoulos, A physics-based approach to modeling real-fuel combustion chemistry – I. Evidence from experiments, and thermodynamic, chemical kinetic and statistical considerations, Combust. Flame 193 (2018) 502–519.

[10] R. Xu, K. Wang, S. Banerjee, J. Shao, T. Parise, Y. Zhu, S. Wang, A. Movaghar, D.J. Lee, R. Zhao, X. Han, Y. Gao, T. Lu, K. Brezinsky, F.N. Egolfopoulos, D.F. Davidson, R.K. Hanson, C.T. Bowman, H. Wang, A physics-based approach to modeling real-fuel combustion chemistry – II. Reaction kinetic models of jet and rocket fuels, Combust. Flame 193 (2018) 520–537.
[11] E. Ranzi, T. Faravelli, P. Gaffuri, A. Sogaro, Low-temperature combustion: automatic generation of primary oxidation reactions and lumping procedures, Combust. Flame 102 (1995) 179–192.
[12] E. Ranzi, M. Dente, A. Goldaniga, G. Bozzano, T. Faravelli, Lumping procedures in detailed kinetic modeling of gasification, pyrolysis, partial oxidation and combustion of hydrocarbon mixtures, Prog. Energy Combust. Sci. 27 (2001) 99–139.
[13] A. Stagni, A. Cuoci, A. Frassoldati, T. Faravelli, E. Ranzi, Lumping and reduction of detailed kinetic schemes: an effective coupling, Ind. Eng. Chem. Res. 53 (2013) 9004–9016.
[14] L. Esclapez, P.C. Ma, E. Mayhew, R. Xu, S. Stouffer, T. Lee, H. Wang, M. Ihme, Fuel effects on lean blow-out in a realistic gas turbine combustor, Combust. Flame 181 (2017) 82–99.
[15] A. Felden, L. Esclapez, Riber, H. Wang, B. Cuenot, Including real fuel chemistry in large-eddy simulations, Combust. Flame 193 (2018) 397–416.
[16] T. Parise, D.F. Davidson, R.K. Hanson, Shock tube/laser absorption measurements of the pyrolysis of a bimodal test fuel, Proc. Combust. Inst. 36 (2017) 281–288.
[17] S. Banerjee, R. Tangko, D.A. Sheen, H. Wang, C.T. Bowman, An experimental and kinetic modeling study of n-dodecane pyrolysis and oxidation, Combust. Flame 163 (2016) 12–30.
[18] Y.L. Wang, A.T. Holley, C. Ji, F.N. Egolfopoulos, T.T. Tsotsis, H.J. Curran, Propagation and extinction of premixed dimethyl-ether/air flames, Proc. Combust. Inst. 32 (2009) 1035–1042.
[19] C. Liu, Z. Li, H. Wang, Drag force and transport property of a small cylinder in free molecule flow: a gas-kinetic theory analysis, Phys. Rev. E 94 (2016) 023102.
[20] C. Liu, W.S. McGivern, J.A. Manion, H. Wang, Theory and experiment of binary diffusion coefficient of n-alkanes in dilute gases, J. Phys. Chem. A 120 (2016) 8065–8074.
[21] C. Liu, R. Zhao, R. Xu, F.N. Egolfopoulos, H. Wang, Binary diffusion coefficients and non-premixed flames extinction of long-chain alkanes, Proc. Combust. Inst. 36 (2017) 1523–1530.
[22] H. Wang, X. You, A. Joshi, S.G. Davis, A. Laskin, F.N. Egolfopoulos, C.K. Law, USC Mech Version II. High-temperature combustion reaction model of H_2/CO/C_1-C_4 Compounds. http://ignis.usc.edu/USC_Mech_II.htm.
[23] R.J. Kee, F.M. Rupley, J.A. Miller, CHEMKIN: A general-purpose, problem-independent, transportable, FORTRAN chemical kinetics code package, Sandia Report SAND-89-8009, Sandia National Laboratories, Albuquerque, N.M., 1989.
[24] R.J. Kee, J.F. Grcar, M.D. Smooke, J. Miller, E. Meeks, PREMIX: a Fortran program for modeling steady laminar one-dimensional premixed flames, Report No. Sandia Report SAND85-8240, Sandia National Laboratories, Albuquerque, NM, 1985.
[25] S.J. Li, A. Campos, D.F. Davidson, R.K. Hanson, Shock tube measurements of branched alkane ignition delay times, Fuel 118 (2014) 398–405.
[26] C.W. Zhou, Y. Li, E. O'Connor, K.P. Somers, S. Thion, C. Keesee, O. Mathieu, E.L. Petersen, T.A. DeVerter, M.A. Oehlschlaeger, G. Kukkadapu, C.J. Sung, M. Alrefae, F. Khaled, A. Farooq, P. Dirrenberger, P.A. Glaude, F. Battin-Leclerc, J. Santner, Y. Ju, T. Held, F.M. Haas, F.L. Dryer, H.J. Curran, A comprehensive experimental and modeling study of isobutene oxidation, Combust. Flame 167 (2016) 353–379.
[27] T. Lu, C.K. Law, Toward accommodating realistic fuel chemistry in large-scale computations, Prog. Energy Combust. Sci. 35 (2009) 192–215.
[28] T. Lu, C.K. Law, A directed relation graph method for mechanism reduction, Proc. Combust. Inst. 30 (2005) 1333–1341.
[29] X. Zheng, T. Lu, C.K. Law, Experimental counterflow ignition temperatures and reaction mechanisms of 1, 3-butadiene, Proc. Combust. Inst. 31 (2007) 367–375.
[30] T. Lu, C.K. Law, A criterion based on computational singular perturbation for the identification of quasi steady state species: a reduced mechanism for methane oxidation with NO chemistry, Combust. Flame 154 (2008) 761–774.
[31] T. Lu, C.K. Law, Systematic approach to obtain analytic solutions of quasi steady state species in reduced mechanisms, J. Phys. Chem. A 110 (2006) 13202–13208.
[32] Z. Ren, S.B. Pope, Entropy production and element conservation in the quasi-steady-state approximation, Combust. Flame 137 (2004) 251–254.